

การสกัดตำแหน่งวัตถุแบบสามมิติจากอินไลน์โฮโลแกรมโดยใช้ค่าสัมประสิทธิ์
ต่ำสุดของการกระจายวิกเนอร์-วิลด์



นางสาวเสาวรส ดาวประทีป

วิทยานิพนธ์นี้เป็นส่วนหนึ่งของการศึกษาตามหลักสูตรปริญญาวิทยาศาสตรมหาบัณฑิต
สาขาวิชาฟิสิกส์
มหาวิทยาลัยเทคโนโลยีสุรนารี
ปีการศึกษา 2558

**EXTRACTION OF 3-D OBJECT POSITION FROM IN-
LINE HOLOGRAMS BY USING MINIMUM
COEFFICIENT OF WIGNER-VILLE
DISTRIBUTION**



**A Thesis Submitted in Partial Fulfillment of the Requirements for the
Degree of Master of Science in Applied Physics
Suranaree University of Technology
Academic Year 2015**

**EXTRACTION OF 3-D OBJECT POSITION FROM IN-LINE
HOLOGRAMS BY USING MINIMUM COEFFICIENT OF
WIGNER-VILLE DISTRIBUTION**

Suranaree University of Technology has approved this thesis submitted in partial fulfillment of the requirements for the Degree of Master.

Thesis Examining Committee

(Asst. Prof. Dr. Worawat Meevasana)

Chairperson

(Prof. Dr. Joewono Widjaja)

Member (Thesis Advisor)

(Asst. Prof. Dr. Panomsak Meemon)

Member

(Dr. Sukanya Tachatraiphop)

Member

(Prof. Dr. Sukit Limpijumnong)

Vice Rector for Academic Affairs
and Innovation

(Prof. Dr. Santi Maensiri)

Dean of Institute of Science

เสาวรส ดาวประทีป : การสกัดตำแหน่งวัตถุแบบสามมิติจากอินไลน์ฮอโลแกรมโดยใช้ค่าสัมประสิทธิ์ต่ำสุดของการกระจายวิกเนอร์-วิลล์ (EXTRACTION OF 3-D OBJECT POSITION FROM IN-LINE HOLOGRAMS BY USING MINIMUM COEFFICIENT OF WIGNER-VILLE DISTRIBUTION) อาจารย์ที่ปรึกษา : ศาสตราจารย์ ดร.ยูโคโน วิชา, 42 หน้า.

วิทยานิพนธ์นี้ได้นำเสนอวิธีการใหม่ในการสกัดตำแหน่งของวัตถุแบบสามมิติจากอินไลน์ฮอโลแกรมโดยใช้การกระจายวิกเนอร์-วิลล์ (ดับเบิลยูวีดี) วิธีการที่นำเสนอนี้มีข้อดีกว่าวิธีแบบมาตรฐานคือไม่เป็นวิธีที่มีการทำซ้ำ ตำแหน่งของวัตถุสามารถสกัดได้โดยปราศจากการสร้างรูปภาพขึ้นใหม่ และการวัดความคมชัดของภาพ ระยะสั้นที่สุดที่สามารถทำการวัดตำแหน่งของวัตถุ กำหนดโดยทฤษฎีการชักตัวอย่างของไนควิส ขณะที่ระยะวัตถุยาวที่สุดขึ้นอยู่กับตำแหน่งต่ำสุดของเปลือกกรอบนอกของสัญญาณฮอโลแกรม และพบว่าสัมประสิทธิ์ดับเบิลยูวีดีของขอบสัญญาณฮอโลแกรมส่วนใหญ่อยู่ตามรีพธแยงมุมซึ่งตัดที่จุดกำเนิดของระนาบดับเบิลยูวีดี ความชันของรีพธแยงมุมนี้แปรผันตรงกับตำแหน่งของวัตถุ หนึ่งในสัมประสิทธิ์มีแอมพลิจูดต่ำสุดเสมอโดยไม่คำนึงถึงตำแหน่งของวัตถุ โดยการตรวจสอบการหาตำแหน่งจากสัมประสิทธิ์นี้สามารถวัดตำแหน่งของวัตถุได้อย่างแม่นยำ ความเป็นไปได้ของวิธีการที่นำเสนอไปนั้นสามารถพิสูจน์ได้จากการยืนยันเชิงการทดลองโดยวิเคราะห์อินไลน์ฮอโลแกรมของไมโครทิวป์ซึ่งมีเส้นผ่าศูนย์กลาง 100 ไมโครเมตร ที่ตำแหน่งต่าง ๆ กัน

สาขาวิชาฟิสิกส์
ปีการศึกษา 2558

ลายมือชื่อนักศึกษา _____
ลายมือชื่ออาจารย์ที่ปรึกษา _____

SAOWAROS DAWPRATEEP : EXTRACTION OF 3-D OBJECT
POSITION FROM IN-LINE HOLOGRAMS BY USING MINIMUM
COEFFICIENT OF WIGNER-VILLE DISTRIBUTION. THESIS ADVISOR
: PROF. JOEWONO WIDJAJA, Ph.D. 42 PP.

DIGITAL HOLOGRAPHY /IN-LINE HOLOGRAMS /OBJECT POSITION
/WIGNER-VILLE DISTRIBUTION

A new method for extraction three-dimensional object position from in-line holograms is proposed by using Wigner-Ville distribution (WVD). The proposed method has an advantage over conventional methods in that it is noniterative. The object position can be extracted without image reconstructions and sharpness measurements. The shortest position that can be measured is determined by the Nyquist sampling theorem, while the longest one depends on a minimum position of the fringe envelope. It is found that the WVD coefficients of a hologram fringe are mainly confined along a diagonal stripe intercepted at the origin of the WVD plane. The slope of this diagonal stripe is proportional to the object position. One of the coefficients always has a minimum amplitude, regardless of the object position. By detecting the position of this coefficient, the object position can be accurately measured. A feasibility of the proposed method is experimentally verified by analyzing the in-line holograms of a microtube with a diameter 100 μm at different positions.

School of Physics

Student's Signature _____

Academic Year 2015

Advisor's Signature _____

ACKNOWLEDGEMENTS

I would like to express my gratitude to the following people for their encouragement, assistance, and support which have enabled me to complete my thesis.

My deepest gratitude goes first and foremost to my thesis advisor Prof. Dr. Joewono Widjaja for his continuous support and advice throughout the study. Without his help, this work would not be possible.

I would like to thank Asst. Prof. Dr. Worawat Meevasana, Asst. Prof. Dr. Panomsak Meemon and Dr. Sukanya Tachatraiphop for serving as at the thesis committee and giving me various excellent advices.

I wish to express my special thanks to the Suranaree University of Technology for financial support through the high potential scholarship (Grant No.1201/2556).

I also would like to thank all lecturers in the School of Physics who have taught and developed my knowledge in the past three academic years. Many thanks are for our research group members, especially Porntip Chuamchaitrakul, for her valuable discussions and suggestions.

Last but not least, I would like to extend my immense gratitude to my parents for their continuous love, understanding, encouragement and support throughout the progress and for motivating me to complete my study.

Saowaros Dawpratee

CONTENTS

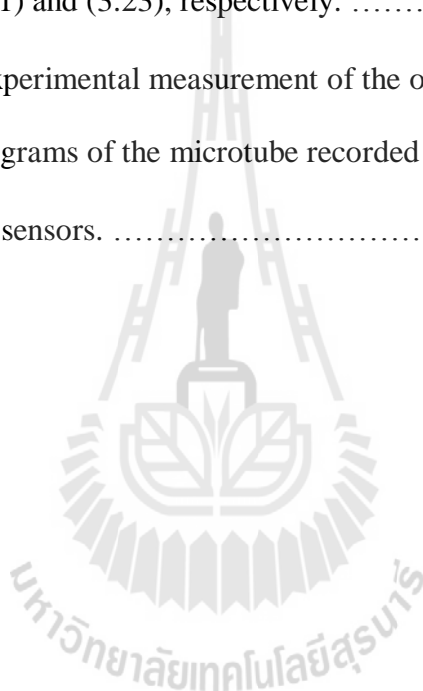
	Page
ABSTRACT IN THAI.....	I
ABSTRACT IN ENGLISH.....	II
ACKNOWLEDGEMENTS.....	III
CONTENTS.....	IV
LIST OF TABLES.....	VI
LIST OF FIGURES.....	VII
CHAPTER	
I INTRODUCTION.....	1
1.1 Background.....	1
1.2 Significance of the study.....	3
1.3 Research objectives.....	4
1.4 Scope and limitation of the study.....	4
1.5 Organization.....	4
II IN-LINE HOLOGRAPHY.....	5
2.1 Digital in-line holography.....	5
2.2 Conventional numerical reconstructions.....	8
2.2.1 Fresnel diffraction integral.....	8
2.2.2 Angular spectrum method.....	10
2.3 Measure of image quality.....	12

CONTENTS (Continued)

	Page
III MATERIALS AND METHODS	14
3.1 Wigner-Ville distribution (WVD)	14
3.2 The WVD of in-line holograms	15
3.3 Extraction of the object position	19
3.3.1 Multiple WVD coefficients	19
3.3.2 Single WVD coefficient with minimum amplitude	19
3.3.3 Algorithm for the position extraction	22
3.3.4 Range of measurements	23
IV EXPERIMENTAL VERIFICATIONS	25
4.1 Hologram formation	25
4.2 Experimental verifications	28
V CONCLUSIONS AND THE FUTURE WORK	36
5.1 Conclusions	36
5.2 Future work	37
REFERENCES	38
CURRICULUM VITAE	42

LIST OF TABLES

Table	Page
4.1 The minimum and the maximum object positions calculated by using Eqs. (3.21) and (3.23), respectively.	26
4.2 Errors in the experimental measurement of the object position from the in-line holograms of the microtube recorded by using the CCD and the CMOS sensors.	34



LIST OF FIGURES

Figure		Page
2.1	A schematic diagram of an optical setup of recording the in-line hologram.	5
2.2	A simulated in-line hologram of a line-shaped object.	6
2.3	An intensity transmittance of the simulated hologram shown in Figure 2.2.	7
2.4	A schematic diagram of the image reconstructions from the in-line hologram $U(\xi, \eta)$	9
2.5	1D cross-sectional scan of image intensity reconstructed from the hologram of the line shaped object at correct recording distance $z = 30$ cm compared with the reconstruction at wrong distances of 20 and 40 cm.	11
2.6	The LAP of any image pixel.	13
3.1	The WVD of the second term of the in-line hologram given by Eq. (2.1) for the positive x axis.	16
3.2	Distribution of $W_{I_{a1}}$, $W_{I_{a32}}$ and $W_{I_{a63}}$ on the WVD plane.	18
3.3	The WVD coefficients calculated by using Eq. (3.10) for $N = 5$ with $a = 50.00$ μm , $z = 10.00$ cm and $\lambda = 543.5$ nm.	19
3.4	1-D plots of the WVD coefficients scanning along the slope.	21
3.5	1-D plots of the 31 st , 32 nd and 33 rd components of WVD.	21

LIST OF FIGURES (Continued)

Figure	Page
3.6	A flow chart for extracting the object position from the in-line hologram with the WVD coefficient with minimum amplitude.23
4.1	An experimental setup for generating the in-line holograms.26
4.2	The microtube mounted on a holder.27
4.3	(a) The in-line hologram of the microtube recorded at the distance $z = 10$ cm and (b) its background intensity.28
4.4	The recorded hologram with the background removal.29
4.5	1-D intensity plot of the hologram shown in Figure 4.4.30
4.6	1-D averaged intensity plot of the hologram shown in Figure 4.5.30
4.7	Comparison of the averaged and the simulated holograms.31
4.8	The WVD outputs of the holograms recorded at the axial distance $z = 10$ cm by using (a) the CCD and (b) the CMOS sensors, respectively.32
4.9	1-D plots of the corresponding WVD coefficients scanned along the slopes of (a) Figure 4.8(a) and (b) Figure 4.8(b), respectively.33

CHAPTER I

INTRODUCTION

1.1 Background

In-line holography is an optical method for recording amplitude and phase of diffracted light wave. When a small opaque object is illuminated by monochromatic light beam, an interference pattern is created by light diffracted by the object light and directly transmitted light (Gabor, 1948). An in-line hologram of the object is produced when the interference pattern is recorded on a photographic film. To optically reconstruct an image of the object, the hologram is illuminated by the same light. In-focus image is reconstructed as same distance as the recording distance.

In particle analysis, conventional in-line holography has been used for studying spatial distribution and size of small objects within a depth of field (Choi and Lee, 2009). In-line particle hologram contains information of the object position which is inversely proportional to a space-varying frequency of the hologram fringe, while a diffraction pattern of the object corresponds to its fringe amplitude.

When an interference pattern of light wave diffracted by an object is digitally recorded by an image sensor array such as charge-coupled device (CCD) (Schnars and Jüptner, 1994; Maxime, Patrick and Gilbert, 2001), an image of the object can be numerically reconstructed from the recorded digital in-line hologram by solving the

Fresnel diffraction integral with fast Fourier transform (FFT) algorithm (Yimo, Qieni and Baozhen, 2004).

Since three-dimensional (3-D) object information can be recorded without modifying appearance and physical characteristic of objects, this interesting property of the in-line holography has been used for solving a focusing problem of monitoring particle and creation of in-focus image from reconstructed images of two object recorded at difference position (Darakis et al., 2010). Studies of circulating flow inside a confined droplet and micro-particle crystallization processes by using digital in-line holography were reported by Seo and Lee (2014) and Khanam (2011), respectively. This digital holographic method was used to study swimming cell in flowing liquid (Moon et al., 2012) and imaging of cancerous tissues (Rong et al., 2015), to name but a few.

To reduce computation time of the FFT, an angular spectrum based numerical method has also been used for the image reconstruction from in-line holograms (Kim, 2010). However in practice, position of objects is unknown information. In order to obtain the in-focus image, a set of images has to be reconstructed at different axial depths with fine intervals. Measure of image quality is then calculated from each reconstructed image in order to obtain the in-focus image. The finer the depth interval, the longer the reconstruction time, however, it gives better accuracy. Therefore, the conventional numerical reconstructions suffer from iteration delay and accuracy problems.

To solve these problems, an extraction of object position from in-line holograms by using Wigner-Ville distribution (WVD) has been proposed (Widjaja

and Chuamchaitrakool, 2013). Unlike the conventional numerical methods, the WVD can directly detect the object position from the holograms. This is because the WVD is a space-frequency signal representation which is useful for measuring local frequency variation. By using the WVD, the obtained local frequency of the fringe can be used to reconstruct the in-focus image without the iterative process.

1.2 Significance of the study

Numerical analysis of the in-line hologram by using the WVD gives output coefficients that are mainly confined along a diagonal stripe intercepted at the origin of the WVD plane. The slope of this stripe is inversely proportional to the object position. In order to measure the object position, all local frequency coefficients appearing on this slope must be determined. The measured object position is calculated by averaging these frequencies.

Among these frequencies, there is a single WVD coefficient which has minimum amplitude, regardless of the object position. The position of the minimum coefficient is exactly on the center of the stripe. Therefore, instead of extracting the position from all WVD coefficients, the use of the single minimum coefficient can reduce further the measurement time of the object position without sacrificing the accuracy.

1.3 Research objectives

- To study theoretically the origin of the WVD coefficient with minimum amplitude.
- To measure the object position from the in-line digital hologram by using the WVD coefficient with minimum amplitude.
- To verify feasibility of the proposed method.

1.4 Scope and limitation of the study

- The test object is a line-shaped object.
- Feasibility of the proposed method is experimentally verified.

1.5 Organization

This thesis consists of five chapters. This is the first chapter which gives an introduction of the thesis. Chapter II reviews fundamentals of digital in-line holography. Numerical methods for image reconstruction and measures of image quality are then discussed. In Chapter III, theory of the WVD is firstly reviewed. Analysis of in-line holograms of a line-shape object by using the WVD is presented and the origin of the WVD coefficient with minimum amplitude is theoretically studied. Chapter IV proposes new algorithm for extracting the object position by using single WVD coefficient with minimum amplitude, which includes its experimental verifications. Finally, the conclusions of the thesis are provided in Chapter V.

CHAPTER II

IN-LINE HOLOGRAPHY

With development of digital image sensors and numerical methods, digital in-line holography have been widely used in the field of science and engineering. An amplitude and phase of diffracted light wave, which is recorded by a CCD sensor, can be numerically reconstructed. In this chapter, fundamentals of digital in-line holography is reviewed. Numerical reconstructions by using the Fresnel diffraction integral and the angular spectrum method are introduced together with the measure of image qualities.

2.1 Digital in-line holography

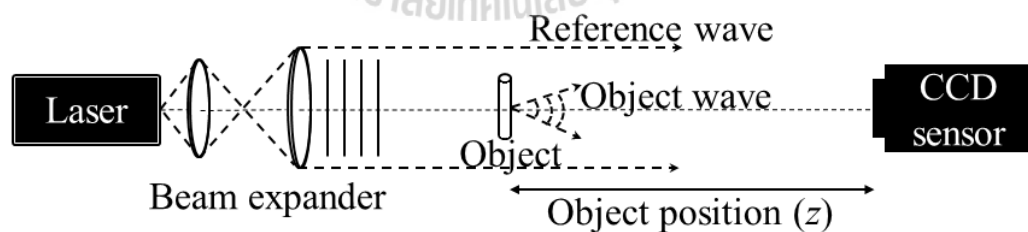


Figure 2.1 A schematic diagram of an optical setup of recording the in-line hologram.

A schematic diagram of an optical setup for recording the in-line hologram of a line-shaped object is shown in Figure 2.1. The object placed along the vertical direction is illuminated by a collimated plane wave generated from a laser source with

a wavelength of λ . The directly transmitted wave and the wave diffracted by the object interfere at the recording plane with a distance z behind the object. When this interference pattern is recorded by a CCD sensor, the in-line hologram of the object is digitally generated.

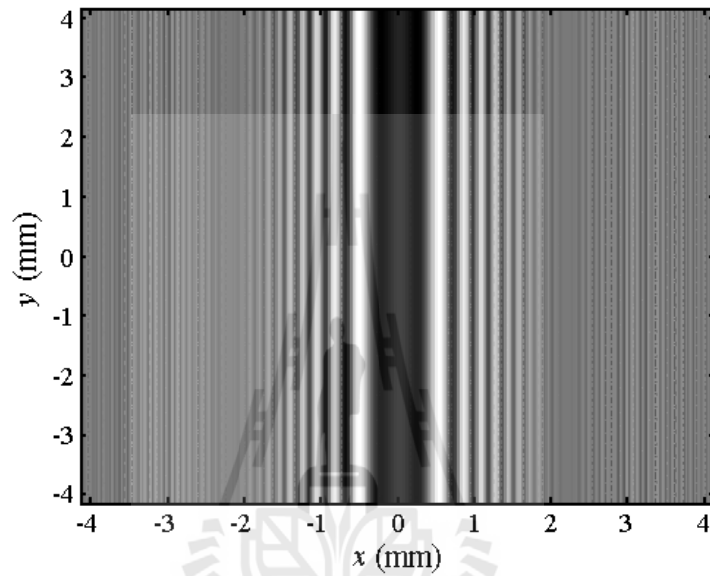


Figure 2.2 A simulated in-line hologram of a line-shaped object.

Figure 2.2 shows the simulated in-line hologram of the line-shaped object with a radius a of $50 \mu\text{m}$ and the recording distance z was 40 cm . The wavelength λ was 534.5 nm , while the length of the recorded signal $2L$ was 8.3 mm . Its intensity transmittance can be expressed as (Tyler and Thompson, 1976)

$$I(x) = \left[1 - \frac{4a}{\sqrt{\lambda z}} \cos\left(\frac{\pi x^2}{\lambda z} - \frac{\pi}{4}\right) \left(\frac{\sin\left(\frac{2\pi ax}{\lambda z}\right)}{\frac{2\pi ax}{\lambda z}}\right) + \frac{4a^2}{\lambda z} \left(\frac{\sin\left(\frac{2\pi ax}{\lambda z}\right)}{\frac{2\pi ax}{\lambda z}}\right)^2 \right] \text{rect}\left(\frac{x}{2L}\right), \quad (2.1)$$

in Eq. (2.1), the first term corresponds to the uniform background of the directly transmitted wave. The second term is the modulation of a cosine chirp function by a sinc function. The diffraction pattern of the line-shape object is represented in the form of the sinc function, while the cosine fringe has the space-varying frequency which is inversely proportional to the recording distance or the object position z . The third term is the square of the sinc function whose amplitude is much smaller than the other terms (Murata, Fujiwara and Asakura, 1970). Consequently, this term can be neglected.

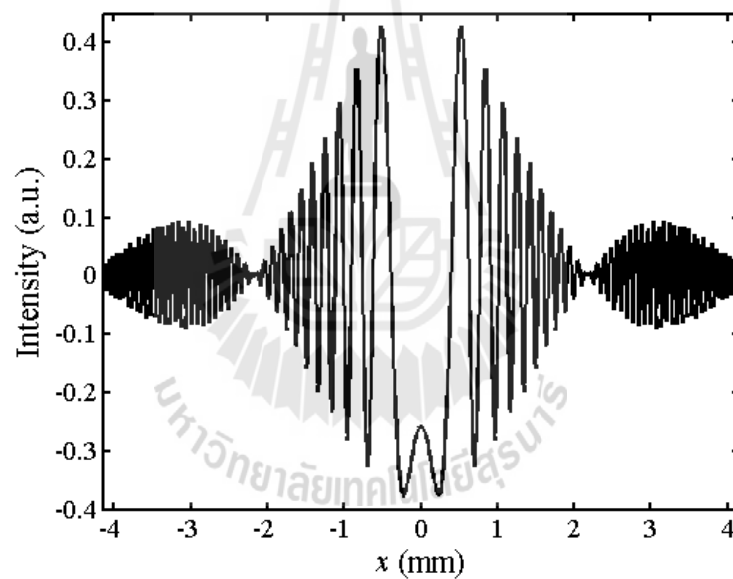


Figure 2.3 An intensity transmittance of the simulated hologram shown in Figure 2.2.

Figure 2.3 shows a plot of a 1D intensity transmittance of the hologram shown in Figure 2.2, which is scanned along the horizontal direction. The space-varying fringe frequency caused by the second term of Eq. (2.1) can be clearly observed from this figure. For a shorter recording distance, the frequency of the cosine fringe

increases rapidly. Since spatial resolution of image sensor is limited, this hologram maybe under sampled. This is the limitation from the digital holography.

2.2 Conventional numerical reconstructions

To extract information from digital holograms, there are two conventional methods, which are widely employed. The first numerical method is the Fresnel diffraction integral, while the second one employs the angular spectrum method.

2.2.1 Fresnel diffraction integral

The Fresnel diffraction integral is a mathematical representation for calculating diffraction due to bending of optical waves around edges of an aperture or an opaque object. The Fresnel diffraction integral is mathematically defined as (Goodman, 1996)

$$U(x, y) = \frac{\exp(jkz)}{j\lambda z} \int_{-\infty}^{\infty} \int_{-\infty}^{\infty} U(\xi, \eta) \exp(j \frac{k}{2z} ((x - \xi)^2 + (y - \eta)^2)) d\xi d\eta, \quad (2.2)$$

where $U(\xi, \eta)$ is the complex optical field just behind a diffracting object located at the (ξ, η) plane, while $U(x, y)$ is the field across the (x, y) plane which is parallel to the (ξ, η) plane with a spatial separation of z . Equation (2.2) can be rewritten as

$$U(x, y) = \int_{-\infty}^{\infty} \int_{-\infty}^{\infty} U(\xi, \eta) h(x - \xi, y - \eta) d\xi d\eta \quad (2.3)$$

with $h(x, y)$ is the impulse response of the wave propagation through free-space given by

$$h(x, y) = \frac{\exp(jkz)}{j\lambda z} \exp\left[\frac{jk}{2z}(x^2 + y^2)\right] \quad (2.4)$$

and the wave number $k = 2\pi / \lambda$.

Figure 2.4 shows a schematic diagram of an optical setup for the image reconstruction from the hologram. Since the hologram is formed by waves diffracted by the object, the hologram needs to be illuminated by same plane wave used in the recording process. The reconstructed wave field is generated behind the hologram. When the object position is unknown, a set of images need to be reconstructed at the different distances. The reconstruction distance producing the in-focus image associates with the correct object position. In Eq. (2.3), $U(\xi, \eta)$ and $U(x, y)$ now represent the wave fields of the hologram and the reconstructed image, respectively.

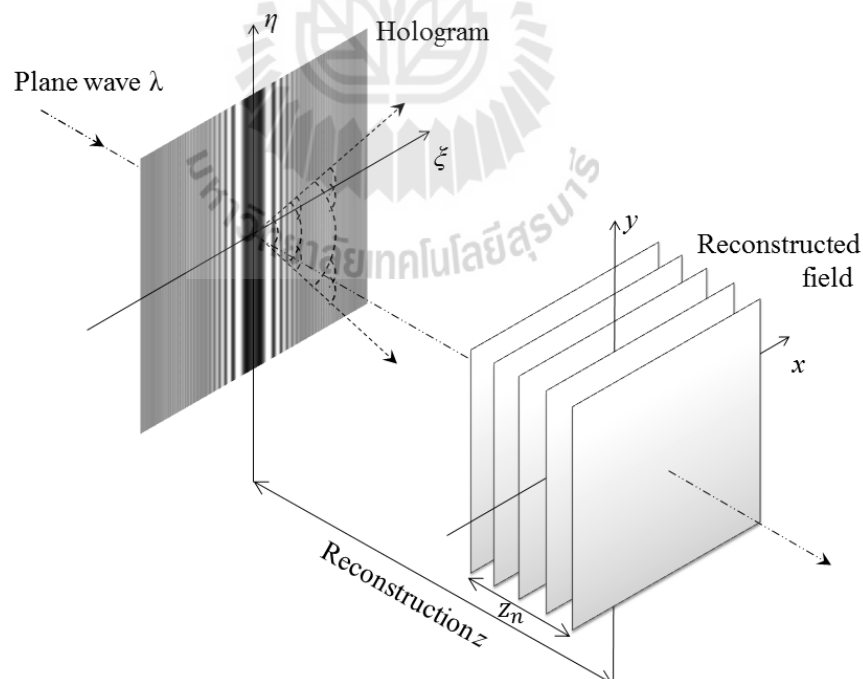


Figure 2.4 A schematic diagram of the image reconstructions from the in-line hologram $U(\xi, \eta)$.

By taking a convolution property of the Fourier transform into account, Eq. (2.3) can be calculated as (Sang et al., 2011)

$$U(x, y) = \mathfrak{F}^{-1} \{ \mathfrak{F} \{ U(x, y) \} \mathfrak{F} \{ h(x, y) \} \}, \quad (2.5)$$

where \mathfrak{F} and \mathfrak{F}^{-1} denote the Fourier transform and its inverse transform, respectively. Due to three Fourier transformations are performed for each image reconstruction, extracting the object position by searching the in-focus image requires considerable amount of time.

2.2.2 Angular spectrum method

In order to reduce the image reconstruction time, use of the angular spectrum method has been proposed (Hazar, Mert and Meric, 2013). In this method, the impulse response of the propagation through free space is directly expressed in the Fourier domain as

$$H(f_x, f_y) = \mathfrak{F} \{ h(x, y) \} = \begin{cases} \exp\left(\frac{j2\pi z_n}{\lambda}\right) \sqrt{1 - (\lambda f_x)^2 - (\lambda f_y)^2} & \sqrt{f_x^2 + f_y^2} < \frac{1}{\lambda} \\ 0 & \text{otherwise.} \end{cases} \quad (2.6)$$

Equation (2.6) is known as the transfer function of the wave propagation phenomenon. Outside a circular boundary of radius $1/\lambda$ in the frequency plane, wave components are rapidly attenuated. The reconstructed wave field can now be calculated as

$$U(x, y) = \mathfrak{F}^{-1} \{ \mathfrak{F} \{ U(x, y) \} \cdot H(f_x, f_y) \}. \quad (2.7)$$

Comparison between the two methods shows that they can reconstruct the same wave field. However, the angular spectrum method saves computation time of the Fourier transformation.

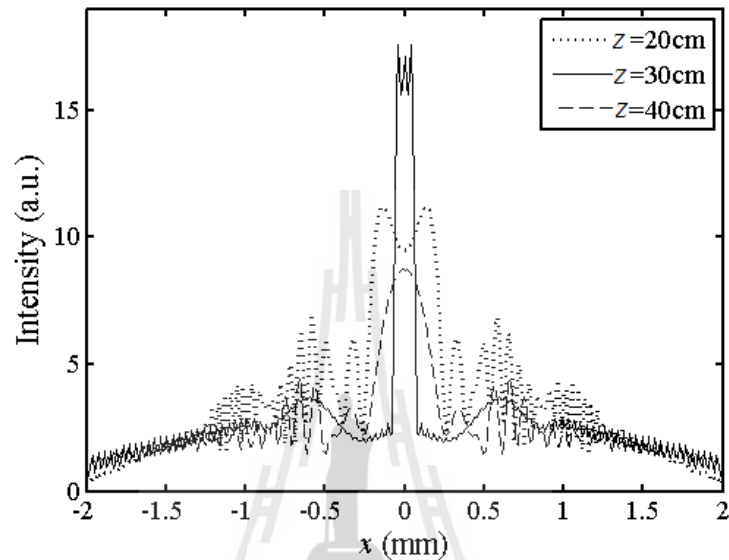


Figure 2.5 1D cross-sectional scan of image intensity reconstructed from the hologram of the line shaped object at correct recording distance $z = 30$ cm compared with the reconstruction at wrong distances of 20 and 40 cm.

Figure 2.5 shows comparisons between the reconstructed image at the distance $z = 20, 30$ and 40 cm. For the recording position 30 cm, the reconstruction gives correct object diameter and the averaged intensity higher than the other images. However, to determine the correct object position from the reconstructed image, the conventional method measures the sharpness quality.

2.3 Measure of image quality

Even though the two numerical methods are useful for reconstructing amplitude and phase of the object wave from the hologram, there is only a single image reconstructed at the desired object position which has the best focus. Therefore, the object position can be measured by evaluating the image sharpness of a set of the reconstructed images. One of useful measures of the image sharpness is Laplace operator (LAP), because its depth of focus is narrowest.

LAP measures variation of intensity gradient of the image reconstructed at the distance z . The LAP operator is defined as (Choi and Lee, 2009)

$$\text{LAP}(z) = \sum_x \sum_y \{\nabla^2 I(x, y, z)\}^2, \quad (2.8)$$

where ∇^2 is the discrete Laplacian operator and $I(x, y)$ is the reconstructed image intensity. For any pixel (x, y) shown in Figure 2.6, the LAP is calculated as

$$\text{LAP}(z) = \sum_{x=1}^M \sum_{y=1}^N [I(x+1, y) + I(x-1, y) + I(x, y+1) + I(x, y-1) - 4I(x, y)]^2 \quad (2.9)$$

with M and N are the number of pixels in the x and the y directions, respectively. By applying the LAP to the image whole pixels, the focus measure of the reconstructed image can be quantitatively evaluated. At the correct object position, the LAP gives maximum value because the object image is sharpest. Since it is able to detect high-frequency edges in the image by neglecting other parts with constant intensity gradient, the LAP has the narrowest depth of focus (Seo and Lee, 2014).

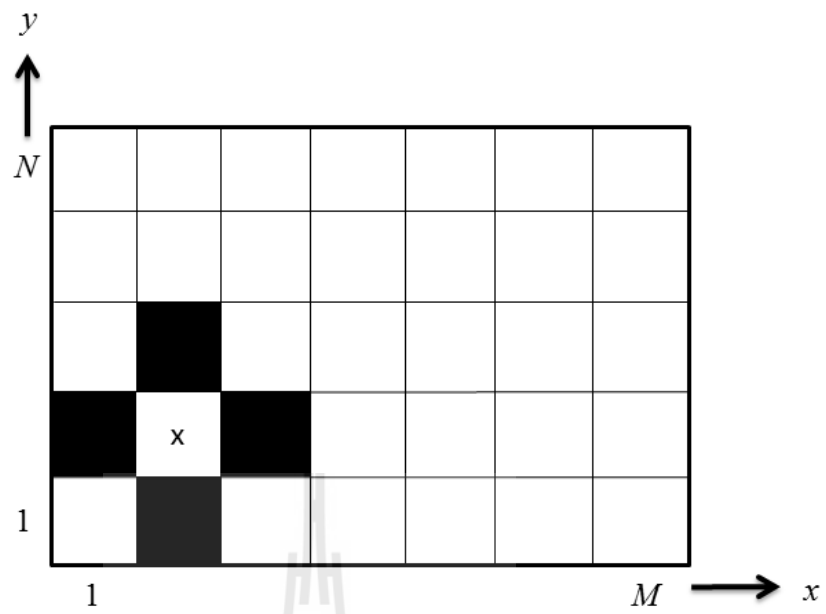


Figure 2.6 The LAP of any image pixel.



CHAPTER III

MATERIALS AND METHODS

This chapter proposes the WVD for solving the limitations of the conventional numerical reconstruction in measuring the object position from in-line holograms. A theoretical background of the WVD is firstly introduced. The discussion is followed by the WVD analysis of the hologram of a line-shaped object. After interpreting the resultant WVD coefficients, an algorithm for extracting the object position by using a single WVD coefficient with minimum amplitude is proposed.

3.1 Wigner-Ville distribution (WVD)

The WVD was first introduced in quantum mechanics by Eugene Wigner in 1932 (Wigner, 1932) and implemented in signal processing by Ville (Ville, 1948). It has been widely used for non-stationary signal analysis, where a conventional Fourier transform fails to provide local frequency spectrum of signal being analyzed. The WVD of an analytic signal $g(x)$ is given by (Boashash, 1988)

$$W_g(x, f_x) = \int_{-\infty}^{\infty} g(x + \tau/2)g^*(x - \tau/2)\exp(-j2\pi f_x \tau)d\tau, \quad (3.1)$$

which can be interpreted as a Fourier transform of an instantaneous autocorrelation $g(x + \tau/2)g^*(x - \tau/2)$. Throughout this thesis $*$ denotes complex conjugation, while the analytic signal $g(x)$ is associated with the real signal $s(x)$ according to

$$g(x) = s(x) + jH[s(x)], \quad (3.2)$$

here, $H[\cdot]$ stands for the Hilbert transform (Abeysekera and Boashash, 1991). In signal processing, the Hilbert transform gives a harmonic conjugate of the signal $s(x)$. It shifts the phase of the positive frequency components of $s(x)$ by $-\pi/2$ radians and the phase of the negative frequency components by $+\pi/2$ radians. In the second term, the product $jH[s(x)]$ restores the positive frequency components and negates the negative frequency components. Consequently, the analytic signal $g(x)$ has only the non-negative spatial-frequency components of $S(f_x)$

$$G(f_x) = \begin{cases} 2S(f_x) & f > 0 \\ S(f_x) & f = 0 \\ 0 & f < 0, \end{cases} \quad (3.3)$$

for this reason the WVD does not suffer from low-frequency artifacts as Wigner distribution function does (Boashash, 1988 and Kadambe, 1992).

3.2 The WVD of in-line holograms

Figure 3.1 shows the plot of the WVD of the second term of Eq. (2.1). The vertical axis represents the spatial-frequency f_x , while the horizontal one is the spatial position x . The WVD coefficients are mainly concentrated in a stripe area,

whose orientation depends on the object position z such as the shorter the distance z , the steeper the slope. These coefficients correspond to the local frequencies of the fringe, which vary linearly with respect to the spatial position.

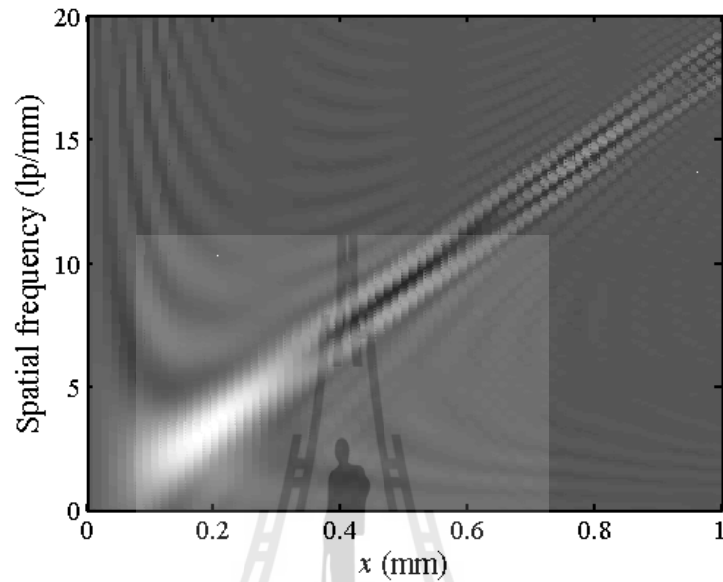


Figure 3.1 The WVD of the second term of the in-line hologram given by Eq. (2.1) for the positive x axis.

In order to have a better insight into the resultant WVD coefficients shown in Figure 3.1, the hologram expression given by of Eq. (2.1) is simplified as

$$I_a(x) = \cos\left(\frac{\pi x^2}{\lambda z} - \frac{\pi}{4}\right) \left[\frac{\sin\left(\frac{2\pi ax}{\lambda z}\right)}{\frac{2\pi ax}{\lambda z}} \right] \text{rect}\left(\frac{x - L/2}{L}\right). \quad (3.4)$$

Mathematical derivation of the WVD of the simplified hologram is done by approximating the sinc function of Eq. (3.4) with a product of N cosine functions (Morrison, 1995)

$$\text{sinc}(2f_0x) = \prod_{n=1}^N \cos\left(\frac{2\pi f_0 x}{2^n}\right). \quad (3.5)$$

The resultant WVD of the approximated Eq. (3.4) is equal to (Chuumchaitrakool, Widjaja and Yoshimura, 2015)

$$W_{I_a}(x, f_x) = \sum_{k=1}^{2^{N+1}-1} \left[\sum_{m=1}^k (-1)^m + \sum_n \cos\left\{ 2\pi f_0 \left[\frac{2^{N+1} - 2(|2^N - n| + 1)}{2^N} \right] x \right\} \right] \\ \times 2(L - 2|x - L/2|) \text{sinc}\left\{ 2(L - 2|x - L/2|) \left[f_x - \left(\frac{2^N - k}{2^N} \right) f_0 - \beta x \right] \right\}, \quad (3.6)$$

where $\beta = 1/\lambda z$ and $f_0 = a/\lambda z$. The maximum number of the WVD components is equal to $2^{N+1}-1$. For $N = 5$, there are 63 components of the WVD which appear along the same slope in the WVD plane. In Eq. (3.6), the characteristics of the WVD of the simplified in-line hologram are as followed. First, each component of the WVD equals to the product of two functions that are the spatial cosine function and the 2-D sinc function of the space and the spatial frequency. Second, the sinc function is modulated by the triangular function with the width equals to the hologram length. Its spatial frequency is determined by β and f_0 . Therefore, the WVD coefficients of the in-line hologram appear along a positive slope shown in Figure 3.1.

Figure 3.2 shows the 3-D plot of the $W_{I_{a1}}$, $W_{I_{a32}}$ and $W_{I_{a63}}$ of the simplified in-line hologram given by Eq. (3.6) for $N = 5$, $a = 2500$ um and $z = 40.00$ cm. The 1st and the 63rd components of the WVD have identical expression

$$W_{I_{a1}}(x, f_x) = 2(L - 2|x - L/2|) \text{sinc}(2(L - 2|x - L/2|)(f - f_0 - \beta x)) \quad (3.7)$$

and

$$W_{I_{a63}}(x, f_x) = 2(L - 2|x - L/2|)\text{sinc}(2(L - 2)|x - L/2|(f + f_0 - \beta x)), \quad (3.8)$$

respectively. They appear at the upper and the lower of the stripe and are separated by $2f_0$ in the spatial frequency direction. The 32nd component of the WVD can be written as

$$W_{I_{a32}}(x, f_x) = \sum_n \cos \left\{ 2\pi f_0 \left[2 - \frac{(2^5 - n + 1)}{2^4} \right] x \right\} \\ \times 2(L - 2|x - L/2|)\text{sinc}\{2(L - 2|x - L/2|)[f_x - \beta x]\}, \quad (3.9)$$

where n is 2, 4, 6, ..., 32. It constitutes of a summation of 16 cosine functions. This WVD component intercepts the origin on the WVD plane.

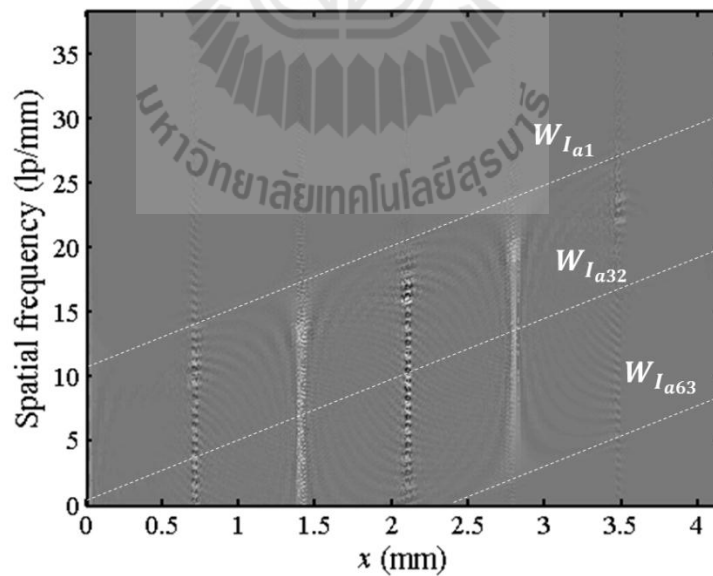


Figure 3.2 Distribution of $W_{I_{a1}}$, $W_{I_{a32}}$ and $W_{I_{a63}}$ on the WVD plane.

3.3 Extraction of the object position

3.3.1 Multiple WVD coefficients

In our previous work, the object position is extracted by using all WVD coefficients appeared along the diagonal stripe intercepted at the origin by using

$$z = x / \lambda f_x. \quad (3.10)$$

The measured position is the average value of the Eq. (3.10) calculated from all desired WVD coefficients. Since this stripe has finite width, it contains multiple WVD coefficients with different amplitude. Consequently, it is hard to select the WVD coefficient, which is exactly appeared along the slope in the middle of the stripe.

3.3.2 Single WVD coefficient with minimum amplitude

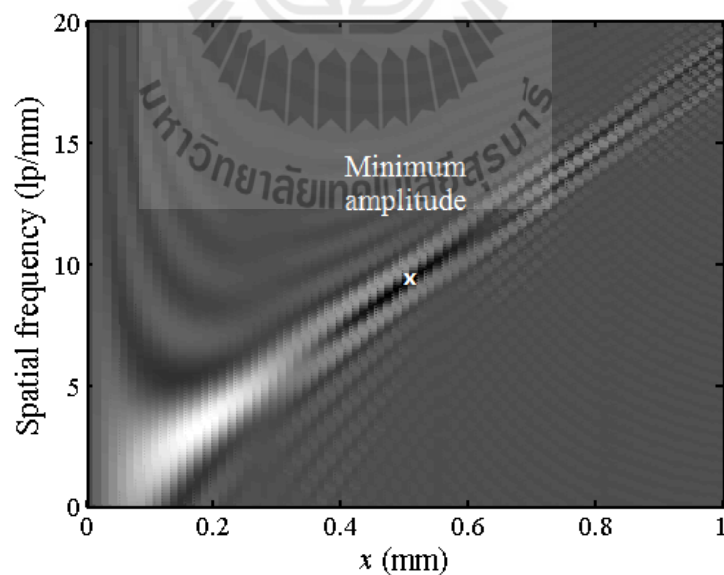


Figure 3.3 The WVD coefficients calculated by using Eq. (3.9) for $N = 5$ with $a = 50.00 \mu\text{m}$, $z = 10.00 \text{ cm}$ and $\lambda = 543.5 \text{ nm}$.

Figure 3.3 shows the WVD calculated by using Eq. (3.9) for $N = 5$ with the same factors a , λ and z . In comparison with Figure 3.1, it is clear that the WVD coefficients appear along the same slope in the WVD plane. After evaluating amplitude of the WVD coefficients, it is found that from the 63 components of the WVD, there is a single WVD coefficient in the stripe area which has minimum amplitude. This minimum coefficient and the origin of the WVD plane forms a line crossing center of the stripe of the WVD coefficients. Therefore, this minimum coefficient belongs exactly to the 32nd component of the WVD, which occurs along the center of the stripe.

In order to understand the origin of this minimum amplitude, the mathematical expression of $W_{I_{a32}}$ is further simplified. The summation of 16 cosine functions in Eq. (3.9) can be expressed as the product of the cosecant and the sine functions

$$W_{I_{a32}}(x, f_x) = \csc(\pi f_0 x / (8 \times 1.22)) \sin(4\pi f_0 x / 1.22) \\ \times 2(L - 2|x - L/2|) \text{sinc}\{2(L - 2|x - L/2|)(f_x - \beta x)\}. \quad (3.11)$$

This cosecant function has the spatial frequency, which is 32 times smaller than the frequency of the sine function. As the phase of the cosecant function varies from 0 to π , its amplitude nonlinearly decreases from undefined value. Therefore, it attenuates the amplitude of the sine function. Since the sinc function corresponds to a broad envelope, therefore, the minimum WVD coefficient is mainly caused by the sine function of Eq. (3.11). This can be verified from Figure. (3.4), which shows the amplitude variations of the WVD coefficients scanned along the slope with the origin as the starting point. The solid line represents the WVD coefficients of Figure 3.1,

while the dotted line is from the 32nd component of the WVD calculated by using Eq. (3.11). It is apparent that the position of the minimum amplitude of $W_{I_{a32}}$ coincides with that of the WVD of Eq. (2.1).

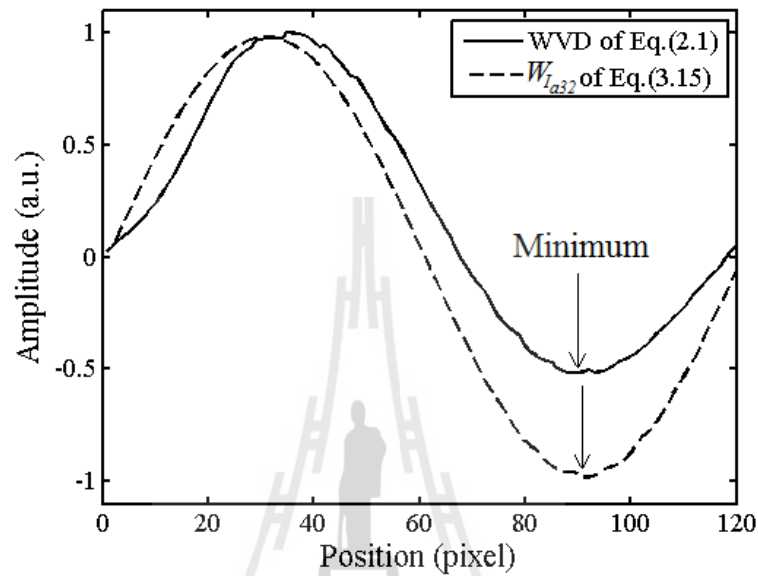


Figure 3.4 1-D plots of the WVD coefficients scanning along the slope.

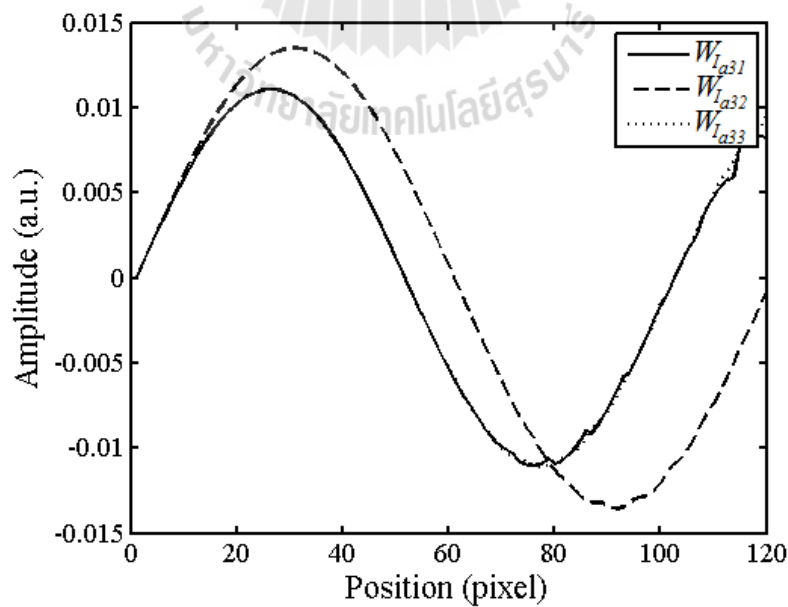


Figure 3.5 1-D plots of the 31st, 32nd and 33rd components of WVD.

Figure 3.5 shows amplitude variations of the 31st, 32nd and 33rd components of the WVD scanned along the slope. They are calculated by using Eq. (3.9) and represented by the solid, the dashed and dotted lines, respectively. In comparison with the other two components, the 32nd component has the lowest amplitude. Therefore, it can be concluded that the sinc function of $W_{I_{a32}}$ is the origin of the minimum amplitude.

3.3.3 Algorithm for the position extraction

This thesis extracts the object position without the needs of the image reconstruction and the sharpness evaluation as the conventional methods do. Our new method for extracting the object position by using a single coefficient of the WVD with the minimum amplitude is done according to the flow chart shown in Figure 3.6. The extraction process starts with generating the analytic signal of the holograms by using Hilbert function of Matlab program. The WVD is computed by taking Fourier transform of the instantaneous autocorrelation of the resultant analytic signal. After finding the coordinate of the WVD coefficient with minimum amplitude, the object position is calculated by

$$\begin{aligned}
 z &= \frac{1}{\lambda} \left(\frac{x_{@min}}{f_{x@min}} \right) \\
 &= \frac{1}{\lambda} \left(\frac{\text{Pixel number of } x@min \times \text{Spatial resolution } \Delta x}{\text{Pixel number of } f_x @ min \times \text{Frequency resolution } \Delta f_x} \right) \quad (3.12)
 \end{aligned}$$

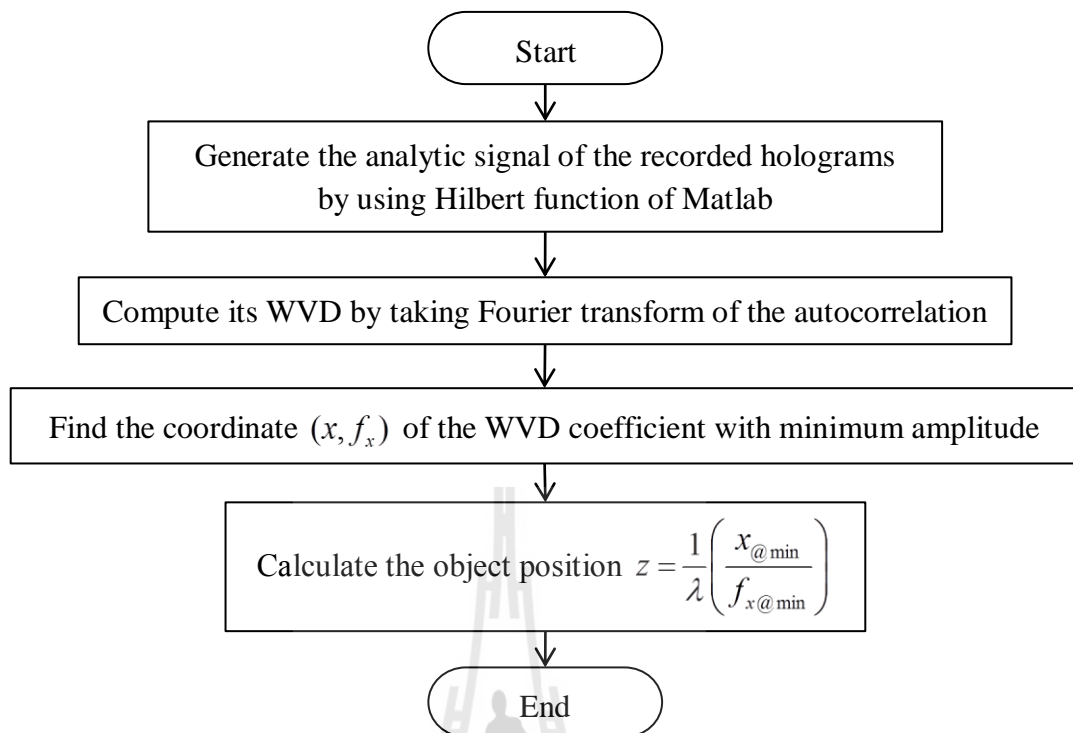


Figure 3.6 A flow chart for extracting the object position from the in-line hologram with the WVD coefficient with minimum amplitude.

3.3.4 Range of measurements

In our proposed method, CMOS and CCD sensors with the size of $L \times L$ and the resolution of $N \times N$ pixels are employed for recording the in-line holograms of the line-shaped object. Due to pixelated structure of these sensors, our proposed method is limited by the finite size and the finite resolution of the sensors. Consequently, in order to record faithfully holograms, the sensors must have the sampling frequency f_{sampling} , which satisfies the Nyquist sampling theorem

$$f_{\text{chip}} < \frac{f_{\text{sampling}}}{2}. \quad (3.13)$$

Note that, the sampling frequency is related to the spatial resolution $\Delta x = L/N$ by

$$f_{\text{sampling}} = \frac{1}{\Delta x}, \quad (3.14)$$

while the hologram fringe has the chirp frequency of

$$f_{\text{chirp}} = x / \lambda z. \quad (3.15)$$

Substitutions Eq. (3.14) and Eq. (3.15) into Eq. (3.13) give

$$\frac{x}{\lambda z} < \frac{N}{L}. \quad (3.16)$$

By considering the minimum analyzable length of the hologram is $x = L/2$, the minimum recording distance can be obtained from Eq. (3.16) as

$$z_{\text{min}} > \frac{L^2}{\lambda N}. \quad (3.17)$$

Furthermore, the theoretical analysis in the proceeding section reveals that the WVD coefficient with the minimum amplitude is determined by the sinc function with the frequency f_0 . This frequency f_0 is related to the object size by $a/\lambda z$. Therefore, in order to be able to detect the minimum amplitude, the holograms must contain information of the object size a . This implies that the first minimum of the sinc function of Eq. (2.1)

$$x = \frac{\lambda z}{2a} \quad (3.18)$$

must be recorded by the sensors. As a result, the minimum recording distance is determined by

$$z_{\text{max}} < \frac{2aL}{\lambda}. \quad (3.19)$$

CHAPTER IV

EXPERIMENTAL VERIFICATIONS

In this chapter, the measurements of the object positions by using the single WVD coefficient with the minimum amplitude were experimentally verified. This experiment took into account effects of sensor resolutions on the proposed measurement. All computations were conducted by using Matlab software version 2009a run on Windows-based notebook.

4.1 Hologram formation

In this study, the holograms of a microtube (Polycarbonate Capillary Tubing / Paradigm Optics) with a radius of 50 μm were simulated by using Eq. (2.1) and experimentally generated by using the coherent plane wave with the wavelength $\lambda = 543.5$ nm. Two image sensors with different spatial resolutions were used to record the holograms. The first sensor was CCD (HAMAMATSU C5948) with the resolution of 640×480 pixels in the area of 8.30×6.40 mm², yielding the spatial resolution $\Delta x = 12.97$ μm . The second one was a CMOS sensor (Beamage 3.0) which had the size of 11.30×6.00 mm² with 2048×1088 pixels. Consequently, the CMOS sensor had 5.51 μm spatial resolution. In order to study effects of the sensor resolutions, the hologram lengths were limited to $L = 4.15$ mm. By taking the spatial

resolutions into account, the maximum and the minimum recording distances can be determined as shown in Table 4.1. The table shows that the CMOS sensor can be used for broader range of the position measurement. On the basis of this measurement range, the holograms of the microtube were recorded at the axial positions of 10, 15, 20, 25, 30, 35 and 40 cm.

Table 4.1 The minimum and the maximum object positions calculated by using Eqs. (3.21) and (3.23), respectively.

sensor	Number of pixel N (pixel)	Length of sensor L (mm)	Minimum position z_{\min} (cm)	Maximum Position z_{\max} (cm)
CCD	320	4.15	9.90	76.36
CMOS	752	4.15	4.21	76.36

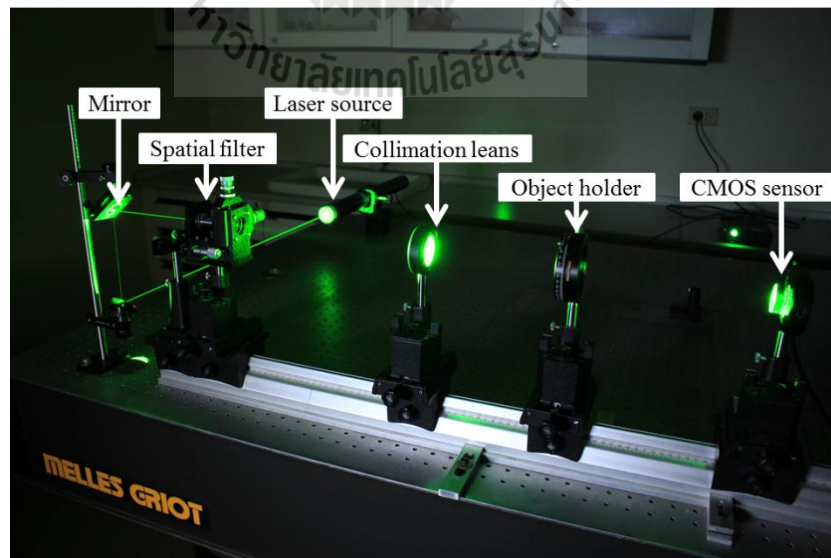


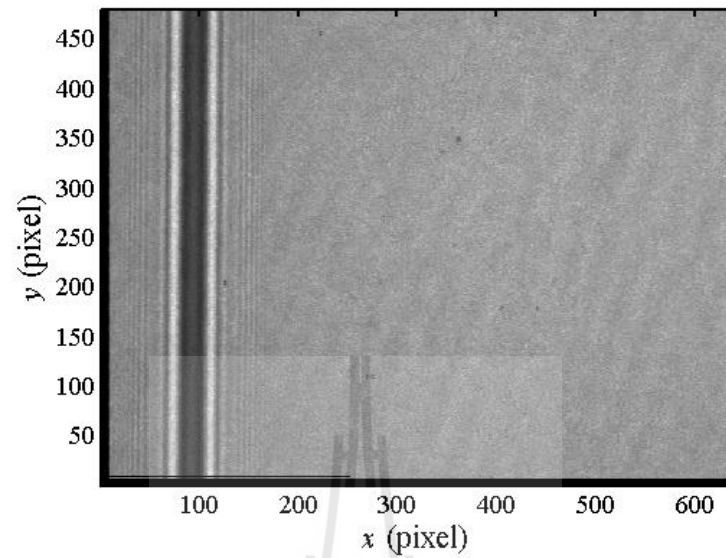
Figure 4.1 An experimental setup for generating the in-line holograms.

Figure 4.1 show an optical setup for recording the Gabor's in-line holograms. After passing through a beam steering device, the light beam was spatially filtered with 50 μm pinhole. The resultant beam was collimated by using a combination of a microscope objective and positive lenses with focal lengths of 9.0 mm and 300 mm. The collimated beam was then used to illuminate the microtube mounted on a rotation holder shown in Figure 4.2.

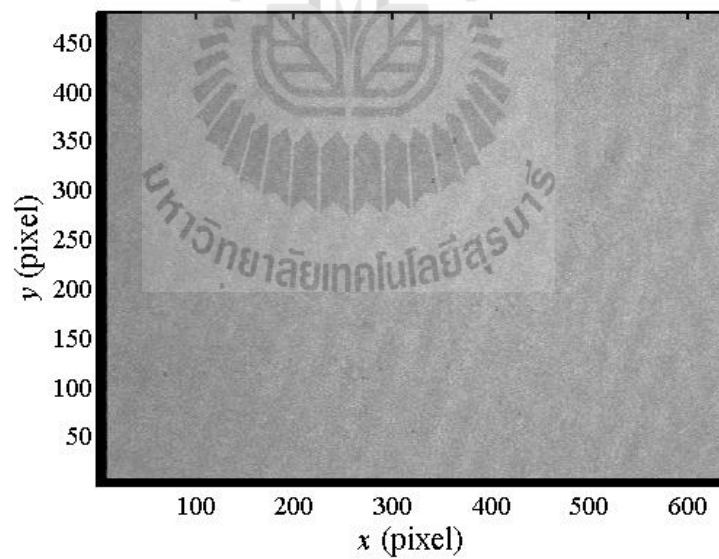


Figure 4.2 The microtube mounted on a holder.

4.2 Experimental verifications



(a)



(b)

Figure 4.3 (a) The in-line hologram of the microtube recorded at the distance $z = 10$ cm and (b) its background intensity.

Figure 4.3(a) show the recorded in-line holograms of the microtube at the recording distance $z = 10$ cm by using the CCD sensor. In order to calculate the WVD of the desired second term of Eq. (2.1), the background intensity shown in Figure 4.3(b) was subtracted from the hologram. This background signal was the intensity of the collimated beam recorded without the object. Figure 4.4 shows the resultant hologram with the background removal. It can be observed from the figure that the unwanted background signal disappears.

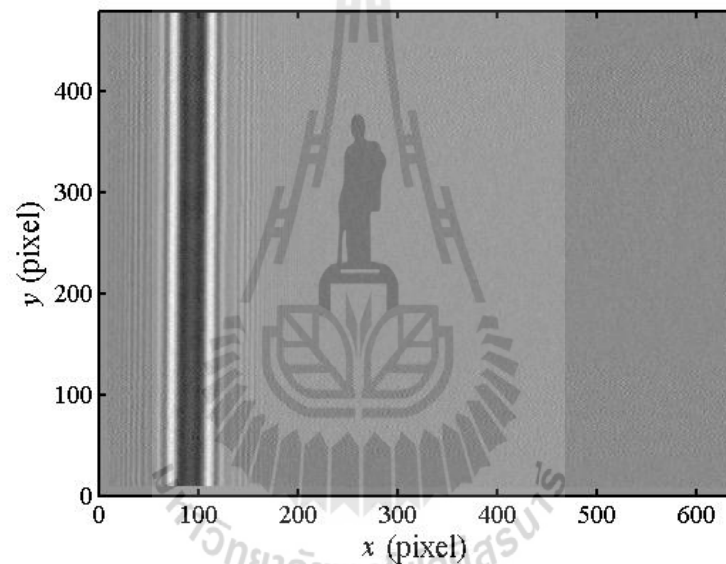


Figure 4.4 The recorded hologram with the background removal.

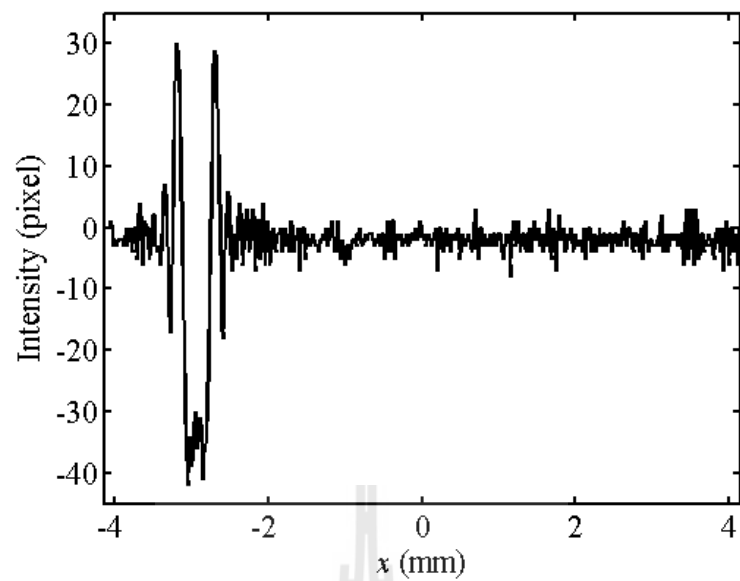


Figure 4.5 1-D intensity plot of the hologram shown in Figure 4.4.

Figure 4.5 show the intensity of the hologram scanned at the 300th row of Figure 4.4. When it is compared with the hologram signal shown in Figure 2.3, it is found that the recorded hologram is noisy due to speckle noise. In order to reduce the speckle noise, the hologram signal was averaged along the vertical direction.

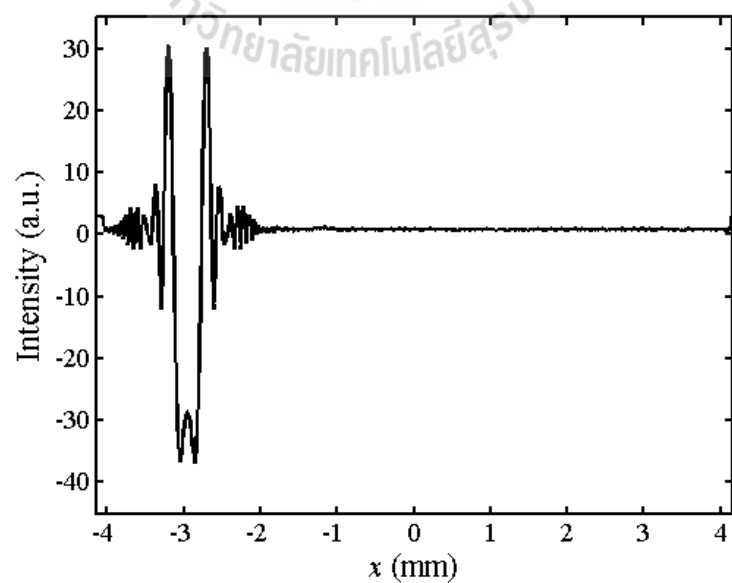


Figure 4.6 1-D averaged intensity plot of the hologram shown in Figure 4.5.

The 1D intensity plot of the averaged hologram signal is shown in Figure 4.6. It is apparent that the noise can be reduced. As shown in Figure 4.7, the averaging process gives the hologram signal as good as the simulated one, because they overlap in low-order sidelobe. The WVD of the resultant hologram signal along the x positive is finally calculated.

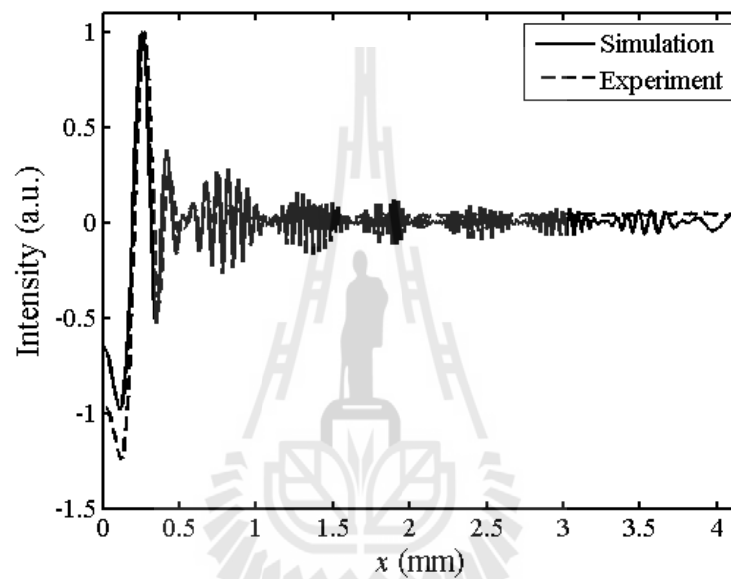


Figure 4.7 Comparison of the averaged and the simulated holograms.

Figures 4.8(a) and (b) show the WVDs of the holograms generated at the distance $z = 10$ cm by using the CCD and the CMOS sensors. Since the spatial and the spatial-frequency resolutions of the sensors are different, the calculated WVD coefficients do not appear at the same slope. 1D plots of the corresponding coefficients scanned along the slope are shown in Figures 4.9(a) and (b), respectively. It is obvious that the WVD coefficients with the minimum amplitudes can be detected from the two figures.

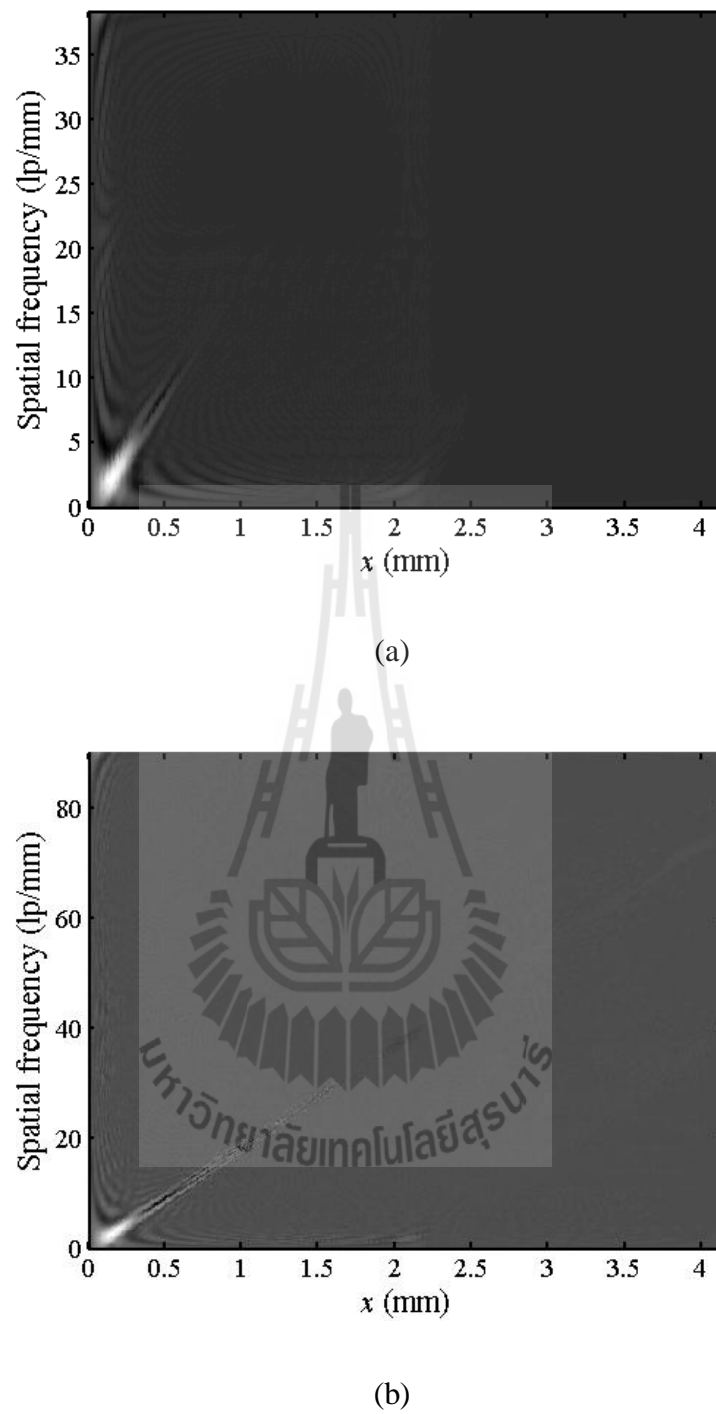
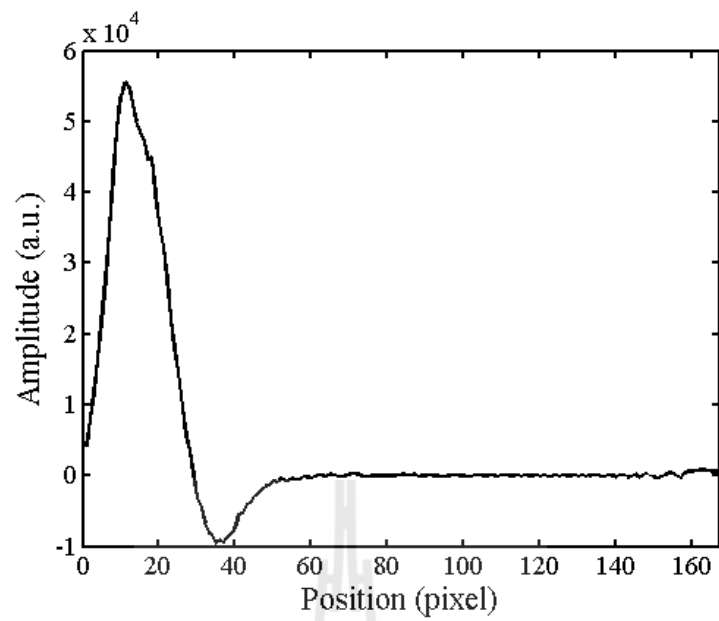
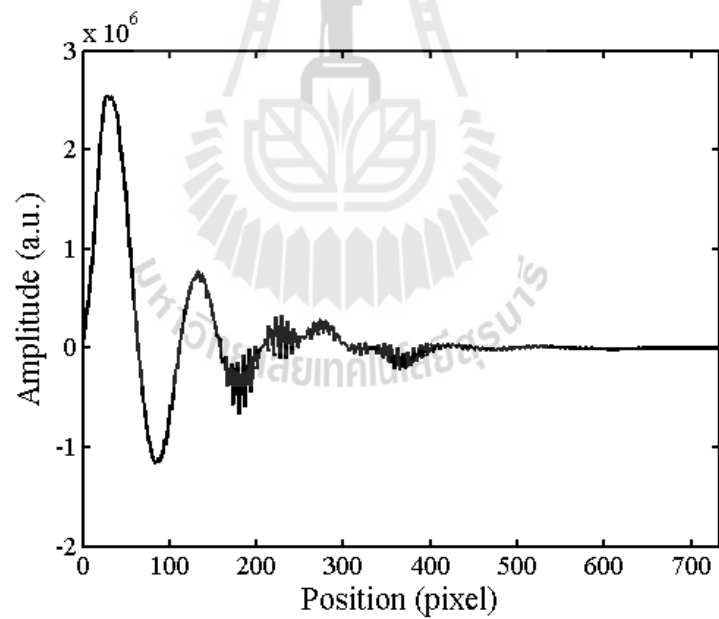


Figure 4.8 The WVD outputs of the holograms recorded at the axial distance $z = 10$ cm by using (a) the CCD and (b) the CMOS sensors, respectively.



(a)



(b)

Figure 4.9 1-D plots of the corresponding WVD coefficients scanned along the slopes of (a) Figure 4.8(a) and (b) Figure 4.8(b), respectively.

Table 4.2 Errors in the experimental measurement of the object position from the in-line holograms of the microtube recorded by the CCD and the CMOS sensors.

Theoretical position z (cm)	CCD sensor				CMOS sensor			
	Coordinate of the WVD minimum		Calculated position z (cm)	Error z (%)	Coordinate of the WVD minimum		Calculated position z (cm)	Error z (%)
	x @ min (pixel)	f_x @ min (pixel)			x @ min (pixel)	f_x @ min (pixel)		
	10.00	35	67	10.27	2.70	84	72	9.89
15.00	53	69	15.24	1.60	128	72	15.14	0.933
20.00	71	70	20.22	1.10	155	71	19.83	0.850
25.00	87	69	25.21	0.840	218	74	25.16	0.640
30.00	107	71	30.18	0.600	261	74	30.14	0.467
35.00	120	69	34.88	0.343	304	74	35.13	0.371
40.00	135	68	39.87	0.325	342	73	40.08	0.200

Table 4.2 presents the errors in measurement of the microtube positions z from the in-line holograms recorded by using the CCD and the CMOS sensors by using the single minimum WVD coefficient. The highest error in measurement is 2.70 % which is obtained from the measurement by using CCD sensor. The error becomes smaller for the longer object position, because the hologram can be more faithfully recorded. It is obvious that the CCD sensor gives higher error than the CMOS, because the spatial and the spatial-frequency resolutions of the CCD is bigger than those of the CMOS sensor. This causes lower accuracy in locating the WVD coefficient with the minimum amplitude.



CHAPTER V

CONCLUSIONS AND THE FUTURE WORK

5.1 Conclusions

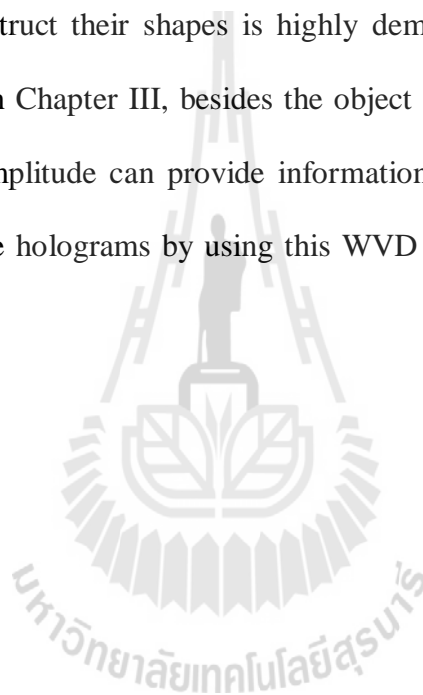
This thesis proposed a new method for extraction object positions from the in-line holograms by using the WVD. Since the hologram fringe encodes the object position into the spatial frequency of the chirp signal, the WVD analysis which provides the local spatial frequency of the fringe can be used for extracting the position information. The significance of this thesis is that the object position can be extracted by using a single WVD coefficient with the minimum amplitude. Therefore, it has an advantage over conventional methods in that it does not require iterative computations of the image reconstruction and the sharpness measurement. Besides the sampling effect which determines the minimum recording distance, this thesis found that the WVD coefficient with the minimum amplitude can be detected, provided the holograms record the minimum point of the envelope function.

In order to study the feasibility of the proposed method, the in-line holograms of the microtube with the diameter of 100 μm were recorded at different axial positions using the CCD and the CMOS image sensors. The proposed WVD analysis was done by using Matlab software version 2009a run on Windows. The experimental results show that the microtube positions can be accurately extracted by using a single computation of the proposed method, provided the sampling effect is minimum. The

error in measurement by using the CCD sensor is higher than that by using the CMOS sensor because its resolutions are lower. Due to the sampling effect, their errors increase as the recording distances become shorter.

5.2 Future work

A single computation method for tracking and sizing small objects together with ability to reconstruct their shapes is highly demanded in diverse microscopic fields. As discussed in Chapter III, besides the object position, the WVD coefficient with the minimum amplitude can provide information of its size. Therefore, object sizing from the in-line holograms by using this WVD coefficient will be studied for further research work.





REFERENCES

REFERENCES

- Abeysekera, S. S. and Boashash, B. (1991). Methods of signal classification using the images produced by the Wigner-Ville distribution. **Pattern Recognition Letters**. 12(11): 717-729.
- Boashash, B. (1988). Note on the use of the Wigner distribution for time-frequency analysis. **IEEE Trans. Acoust. Speech Signal Proc.** 36: 1518-1521.
- Choi, Y. K. and Lee, S. J. (2009). Three-dimensional volumetric measurement of red blood cell motion using digital holographic microscopy. **Appl. Opt.** 48: 2983-2990.
- Chuamchaitrakool, P., Widjaja, J. and Yoshimura, H. (2015). Holographic particle sizing using Wigner-Ville distribution. **Opt. Laser Eng.** 67: 186-190.
- Darakis, E., Khanam, T., Rajendran, A., Kariwala, V., Naughton, T. J. and Asundi, A. K. (2010). Microparticle characterization using digital holography. **Chem. Eng. Sci.** 65(2): 1037-1044.
- Gabor, D. (1948). A new microscopic principle. **Nature**. 161: 77-79.
- Goodman, J. W. (1996). **Introduction to Fourier Optics**.
- Hazar, A. I., Mert, D. and Meric, ö. (2013). Fast autofocusing in digital holography using scaled hologram. **Opt. Communications**. 287: 81-84.
- Julius, O. S. III (2007), **Mathematics of the discrete Fourier transform (DFT) with Audio Applications**.
- Kadambe, S. (1992). A Comparison of the Existence of “Cross Terms” in the Wigner Distribution and the Squared Magnitude of the Wavelet Transform and the Short

- Time Fourier Transform. **IEEE Transactions on Signal Processing**. 40(10): 2498-2517.
- Khanam, T., Rahman, M. N., Rajendran, A., Kariwala, V. and Asundi, A. K. (2011). Accurate size measurement of needle-shaped particles using digital holography. **Chem. Eng. Sci.** 66: 2699-2706.
- Kim, MK. (2010). Principle and techniques of digital holographic microscopy. **J. Photon. Energy**. 0001: 108005-01-50.
- Maxime, J., Patrick, S. and Gilbert, T. (2001). High resolution digital holography. **Opt. Communications**. 190(1): 87-94.
- Moon, I., Javidi, B., Yi, F., Boss, D. and Marquet, P. (2012). Automated statistical quantification of three-dimensional morphology and mean corpuscular hemoglobin of multiple red blood cells. **Opt. Exp.** 20(9): 10295-10309.
- Morrison, KE. (1995). Cosine products. Fourier transforms and random sums. The **American Mathematical Monthly**. 102(8): 716-724.
- Murata, K., Fujiwara, H. and Asakura, T. (1970). Several problems in in-line Fraunhofer holography for bubble-chamber track recording. In Robertson, E.R., Harvey, J.M. (eds.), **Proc. Conf. Engineering Use of Holography**. (pp. 289-300). Cambridge : University Press.
- Rong, L., Latychevskaia, T., Chen, C., Wang, D., Yu, Z., Zhou, X., Li, Z., Huang, H., Wang, Y. and Zhou, Z. (2015). Terahertz in-line digital holography of human hepatocellular carcinoma tissue. **Sci. Rep.** 5: 1-6.
- Sang, J. L., Kyung, W. S., Yong, S. C. and Myong, H. S. (2011). Three-dimensional motion measurements of free-swimming microorganisms using digital holographic microscopy. **Meas. Sci. Technol.** 22(6): 064004-1-8.

- Schnars, U. and Jüptner, W. (1994). Direct recording of holograms by a CCD target and numerical reconstruction. **Appl. Opt.** 33(2): 179-181.
- Seo, W. K. and Lee, S. J. (2014). High-accuracy measurement of depth displacement using a focus function and its cross- correlation in holographic PTV. **Opt. Express.** 22(13): 15542-15553.
- Tyler, G. A. and Thompson, B. J. (1976). Fraunhofer holography applied to particle size analysis: a reassessment. **Opt. Acta.** 23: 685-700.
- Ville, J. (1948). Théorie et Applications de la Notion de Signal Analytique. **Câbles et Tran.** 2: 61-74.
- Widjaja, J. and Chuamchaitrakool, P. (2013). Holographic particle tracking using Wigner-Ville distribution. **Opt. Lasers Eng.** 51: 311-316.
- Wigner, E. (1932). On the quantum correction for the thermodynamic equilibrium. **Physics Reviews.** 40: 749-759.
- Yimo, Z. Qieni, L. and Baozhen, G. (2004). Elimination of zero-order diffraction in digital off-axis holography. **Opt. Communications.** 204(4): 261-267.

CURRICULUM VITAE

Name : Saowaros Dawprateep

Date of Birth : May 11, 1990

Place of Birth : Chaiyaphum, Thailand

Education : B.Sc. Department of Physics, Khon Kaen University,
Thailand, 2013

Publications :

- Dawprateep, S., Widjaja, J., Chuamchaitrakool P. and Meemon, P. (2015).
Properties of Wigner-Ville distribution's coefficients in in-line particle
hologram analysis. **Proc. of SPIE.** 9059: 96590E1-96590E4.

Awards : -

Grants and Fellowships : -

Position and Place of Work : -

Scholarship :

- SUT Scholarships for Potential Graduate Students (Grant no. 1201/2556)